Supergen

Offshore Renewable Energy

Early Career Researcher Posters and Abstracts Booklet

2026 Annual Assembly

Surnames A-B

UKRI Engineering and Physical Sciences Research Council

Early Career Researcher Posters 2026

Abel Arredondo-Galeana, University of Strathclyde Complementary analysis of a wave wind farm for offshore hydrogen production
Elias Arcondoulis, University of Southampton Structured porous media for scour mitigation around offshore foundations
Abid Arham, University of Exeter Coupled Thermal Modelling of Dynamic Submarine Power Cables under Varying Sea Temperatures
Madison Asbury, University of Strathclyde Probabilistic Fatigue Life Assessment of Offshore Wind Structure Accounting for Manufacturing Imperfections
Abigail Bateman, University of Southampton Reliability-based design of offshore wind gravity foundations
Scott Brown, University of Oxford Supergen ORE Hub WS4: Response-conditioned short design events for floating ORE applications

Complementarity analysis of a wave wind farm for offshore hydrogen production.

Dr Abel Arredondo-Galeana[a], Dr Shona Pennock[b], Dr Daniel Nibblet[c], Katarzyna Patryniak[a], Professor Maurizio Collu[a], Professor Feargal Brennan[a]

[a] NAOME, Faculty of Engineering, University of Strathclyde

b CorPower Ocean, Stockholm, Sweden

c Electrochemical Engineering, School of Engineering, University of Newcastle, UK

Engineering and Physical Sciences Research Council

Supergen Offshore Renewable Energy

Wave wind farm

The schematic of a co-located wave–wind farm is depicted in Figure 1. The offshore farm consists of a 5 MW wind turbine mounted on the OC4-DeepCwind semi-submersible platform (Robertson et al., 2014). A total of five single-buoy wave energy converters (WECs), each rated at 400 kW [1], are arranged in front of the floating wind turbine to supply power to a hydrogen plant rated at 5 MW. The diameter (D) of the WECs is 9 meters, and the lateral spacing between devices is $3D$. The back row of WECs is positioned $10D$ upstream of the front pontoon of the platform. Further details of the farm are available via the QR code below.

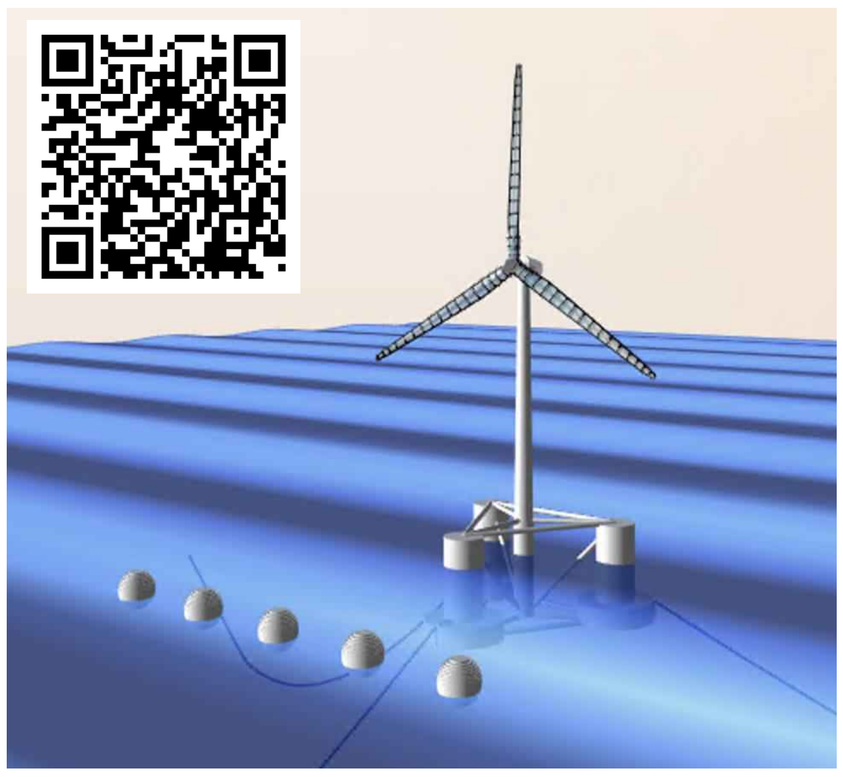

Figure 1– Wind-wave farm array layout with a WEC fence facing the dominant wave direction.

Hydrogen production

The power output of the 5 MW wind turbine, the five wave energy converters (WECs) rated at 400 kW each, and their combined output are shown in Figure 4a using two months of hourly data (January-February 2024). Wind power is shown in black, wave power in red, and the combined output in blue. The results highlight the complementary nature of these resources in swell-dominated regions, where wind and wave conditions exhibit low correlation. The grey regions in Figure 4a indicate periods when wind power drops below a specified power threshold, while wave power (green regions) remains above the threshold, which is set to 1 MW in this case. Additionally, the yellow regions highlight periods when both wind and wave resources are available simultaneously, increasing the overall energy yield. Figure 4b presents the corresponding cumulative hydrogen production. The wind-only case (black) shows intermittent growth, with flat regions during periods of absent wind power. In contrast, the combined system (blue) eliminates these gaps and increases the overall rate of production. Notably, although wave energy has less than half the installed capacity of wind (2 MW vs. 5 MW), its contribution increases hydrogen production by 50% by the end of the two-month period, due to both gap-filling and periods of simultaneous resource availability.

Wave height attenuation

Figure 2a shows the wave surface elevation around the wave farm at a dimensionless time period $T^* = 10.9$ ($\omega = 1.8$ rad/s). The transmission coefficient K_T ,defined as the ratio of downstream to upstream wave height, is used to evaluate wave attenuation for a single WEC and a WEC fence of 10 devices. Figure 2b shows that the multi-WEC configuration demonstrates significantly stronger attenuation, reducing K_T to approximately 0.4 for dimensionless wave periods $10 \leq T^* < 15$,followed by a gradual increase toward $K_T \approx 1$ as T^* increases. A single WEC provides minimal attenuation, with $K_T \approx 0.9$–1 across $10 \leq T^* < 15$. For long wave periods ($T^* \geq 25$), both configurations converge to $K_T \approx 1$,indicating negligible attenuation. Overall, WEC arrays are substantially more effective than individual devices at reducing downstream wave energy, particularly or intermediate wave periods ($10 \leq T^* < 15$).

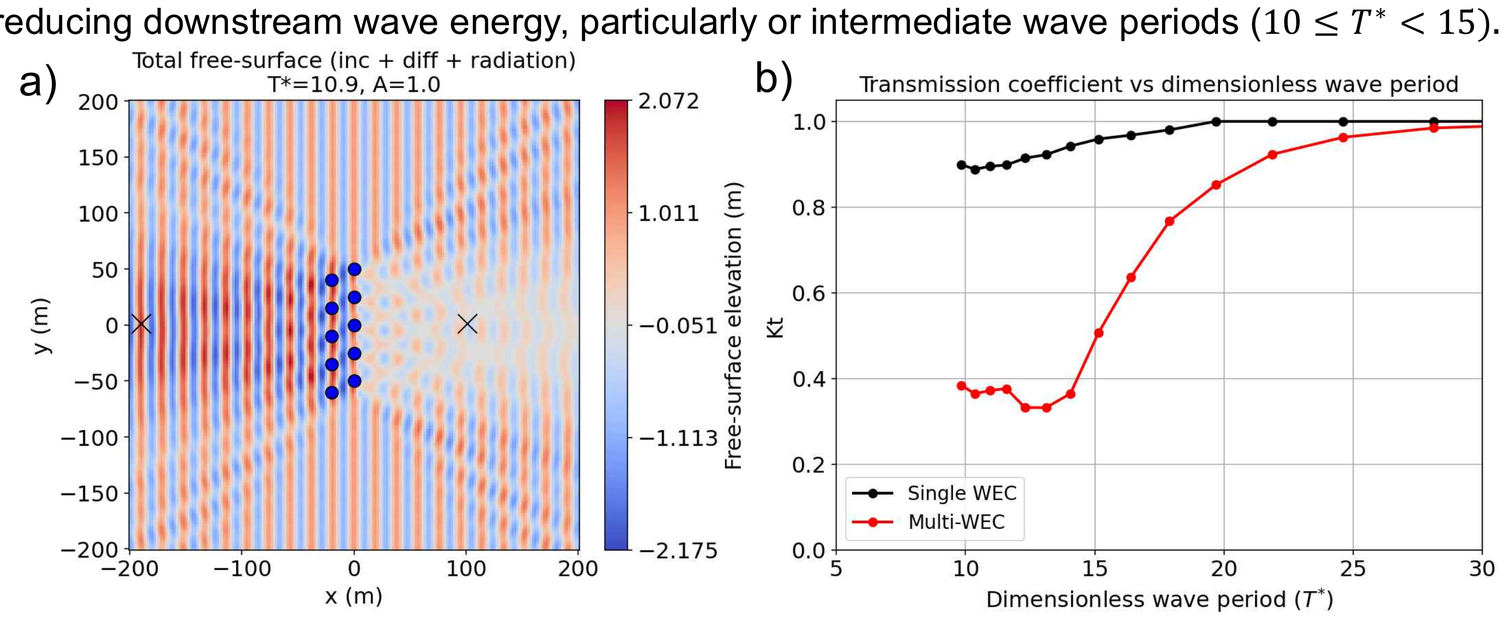

Figure 2 – a) Surface wave elevation around a WEC fence consisting of two rows; b) Transmission coefficient (K_T) for a single WEC and for 10 WECs distributed in two rows.

Wind turbine (WT) controller effort

Figure 3 shows the standard deviation of the aerodynamic (orange markers) and electrical power (blue markers) of the wind turbine at different dimensionless wave periods (T^*). We find that 10 WECs reduce variability in turbine aerodynamic power through wave attenuation over the range of $10 \leq T^* < 15$. However, electrical power variability remains low across all cases ($10 \leq T^* < 35$) due to effective turbine control (blue markers).

This indicates that power quality is governed by the control system rather than wave conditions. Wave attenuation does not directly improve electrical power quality for hydrogen electrolysers. Nevertheless, the reduction in aerodynamic variability implies a lower control effort, as less pitch activity is required to maintain a stable power output. Three regions of control effort are identified in the figure, corresponding to low, medium, and high effort, shown in green, yellow, and red, respectively.

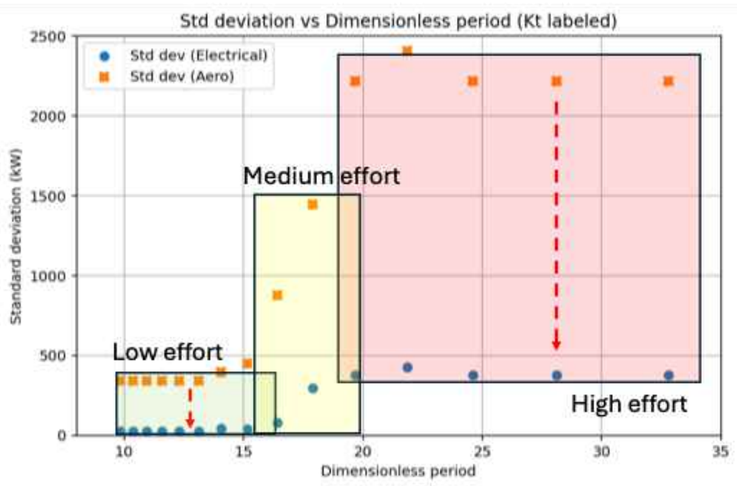

Figure 3 – Standard deviation of aerodynamic and electrical power of WT at different T^*

Figure 4 – a) Power time series of wind, wave, and wind + wave and b) Cumulative hydrogen production from wind only and wind + wave combined.

[1] Blech, E. M. (2023). *Developing a cost model For combined offshore farms: The advantages of co-located wind and wave energy* (Master's thesis, Universitat Politècnica de Catalunya, KTH Department of Technology).

[2] Niblett, D., 2023. powertoelectrolysis. https://github.com/DNiblett/powerToElectrolysis. GitHub repository. Ocean Refuel. University of Newcastle, UK.

Ocean REFuel

University of Strathclyde

Newcastle University

CorPower Ocean

Coupled Thermal Modelling of Dynamic Submarine Power Cables under Varying Sea Temperatures

Abid Arham[1], Philipp R. Thies[1], Ajit C. Pillai[1], Stylianos Koumlis[2]

[1]Renewable Energy, Department of Engineering, University of Exeter, Penryn, UK
[2]Fulgor Single Member S.A, Hellenic Cable Industry, Athens, Greece

Supergen Annual Assembly, University of Warwick , 21 & 22 April 2026

Introduction:

To date, Thermal loads have become one of the primary concerns in submarine power cable design.

- Literatures cover thermal loads on submarine power cable especially on static buried cable.
- Thermal loads on dynamic power cable have not been explored in detail yet.

Exposed dynamic cables is not well covered yet

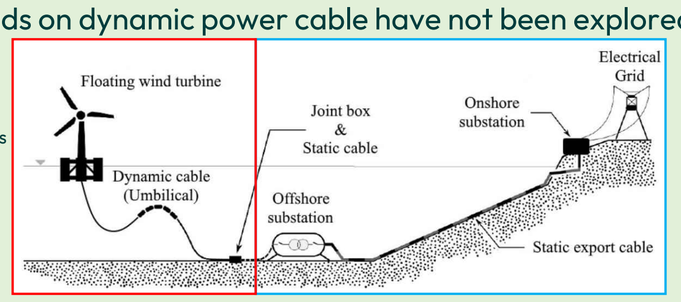

Buried static cables is well covered

Yang et al. (2024), Wang et al. (2020), Rachek and Larbi (2008), Grivas et al. (2020), Ostero et al. (2015), Gonzalez et al. (2021), Matine et al. (2019), Makassi et al (2022)….

IEC standards 60287-1, IEC standards 60287-2, -IEC TR 62095, CIGRE TB 963

Objective:

Assess thermal behaviour of dynamic submarine power cable and evaluate impact of sea temperature on current rating.

Scope:

Steady-state coupled Electromagnetic-Thermal analysis covering a range of sea temperature expected for the planned floating offshore wind farm globally.

Region	Location	Temperature Range			Ref.
		Min (˚C)	Max (˚C)	Average* (°C)	
Europe	North Sea	6	18	7	[8]
	English Chanel	7	16	11	[9]
	Celtic Sea	6	20	11	[10]
	Baltic Sea	4	20	7	[11]
	Mediterranean Sea	5	30	13	[12]
Asia	Taiwan Strait	10	29	15	[13]
	South China Sea	13	33	15	[13]
	Yellow Sea	2	27	13	[14]
	East China Sea	5	30	14	[13]
	Sea of Japan**	0	25	0	[15]
America	East Coast	6	20	10	[16]

* Average sea temperature below the surface layer.
** Sea of Japan is discounted from the analysis due to its unique temperature characteristic.

Model and Methodology:

- Typical 66 kV with properties based on compiled public domain data taken from literatures and supplier specifications. To allow practical modelling on cable layers, several simplifications on thin cable layers are made.
- COMSOL Multiphysics FEA software is used to build a two-dimensional three-core cable model in accordance with IEC standards 60287-1 and 60287-2.
- A set of steady-state analysis considering increased transmission current ranging from 0 A to 1200 A in a 20°C basecase ambient temperature is conducted to find the operational rated current.

Material	Thermal Conductivity (W/mC)	Electrical Conductivity (S/m)	Resistivity (Ω·m)
Copper	401	5.998E+07	1.667E-08
XLPE	0.2857	1.00E-15	1.00E+15
MDPE	0.4	1.00E-13	1.00E+13
HDPE	0.1667	1.00E-16	1.00E+16
PP	0.209	1.00E-14	1.00E+14
Galvanised Steel	44.5	4.03E+06	2.48E-07

Ref: [1], [4], [19], [20]

Typical properties of a three-core 66 kV submarine power cable

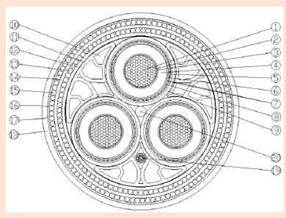

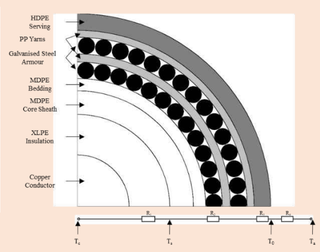

Cable Thermal Resistance

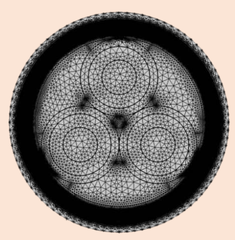

Physic-controlled COMSOL meshing

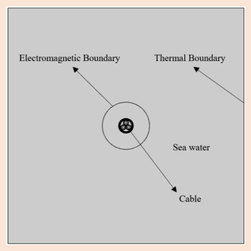

Boundary Conditions

$$I = \left[\frac{\Delta\theta - W_d[0.5R_1 + n(R_2 + R_3 + R_4)]}{R_C R_1 + nR_C(1+\lambda_1)R_2 + nR_C(1+\lambda_1+\lambda_2)(R_3+R_4)}\right]^{0.5}$$

I: Permissible current rating (A)
$\Delta\theta$: Conductor temperature rise above the ambient temperature (K)
W_d : Sielectric loss per unit length of the cable for the insulation surrounding the conductor $\left(\frac{W}{m}\right)$
R_C : Alternating current resistance per unit length of the cable at maximum operating temperature $\left(\frac{\Omega}{m}\right)$
n : Number of load-carrying conductors in the cable
R_1 : Thermal resistance per unit length of cable between one conductor and the sheath $\left(K \cdot \frac{m}{W}\right)$
R_2 : Thermal resistance per unit length of cable between the sheath and armour $\left(K \cdot \frac{m}{W}\right)$
R_3 : Thermal resistance per unit length of cable outer-sheath $\left(K \cdot \frac{m}{W}\right)$
R_4 : Thermal resistance per unit length between the cable surface and the surrounding medium $\left(K \cdot \frac{m}{W}\right)$
λ_1 : Ratio of losses in the metal sheath to total losses in all conductors in the cable
λ_2 : Ratio of losses in the armouring to total losses in all conductors in the cable.

$$\sigma(T) = \frac{1}{\rho_{20}[1 + \alpha_{20}(T-20)]}$$

$$W_d = \omega C U_0{}^2 \tan\delta$$

$\sigma(T)$: Core conductivity.
ρ_{20} : Resistivity of the core material at 20°C $(\Omega \cdot m)$.
α_{20} : Temperature coefficient of resistance of the core material at 20°C $(1/K)$.
T : Temperature (°C).
W_d : Dielectric losses per unit length
C : Capacitance per unit length of cable (F/m)
U_0 : Voltage to earth (V)
$\tan\delta$: Loss factor of the insulation.

Results:

Cable rated current of 903 A at 90°C maximum allowed core operational temperature.

- Match typical specification of 66kV submarine power cable, which has rated current ranging from 700 A to 1100 A.
- Validated against IEC 60287-a and 60287-2 with 3.21% difference on rated current.

Further analysis considering different sea temperatures

- Giving an idea on the limiting operational current needed to keep the cable operating within its core temperature operational limit of 90°C.
- 11.37% knockdown factor on the operational current limit between 5°C and 30°C sea temperature.

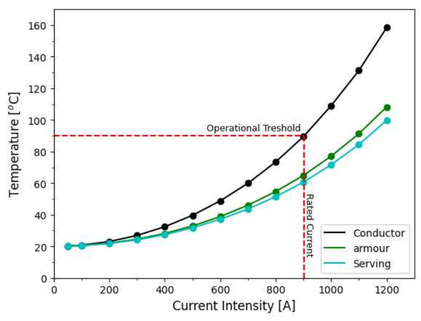

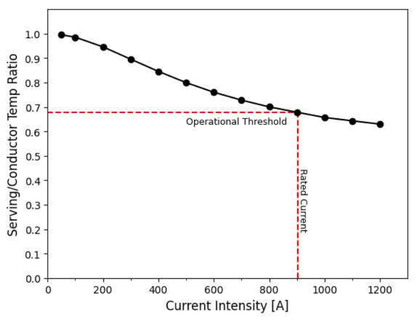

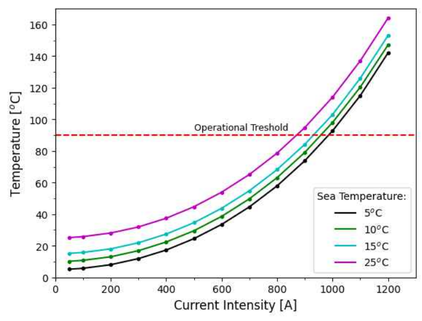

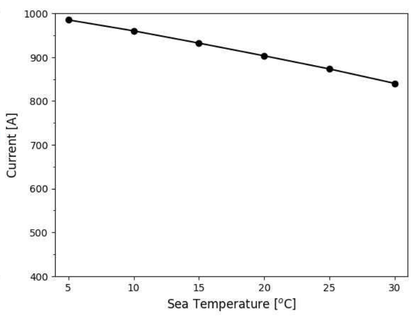

Method	Rated Current (A)
COMSOL FEA	903
Thermal Resistance – IEC 60287	932.95
Difference	3.21%

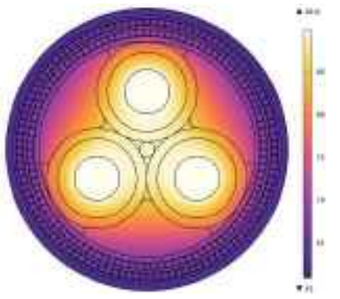

Cable rated current (903 A) at 90°C core operational temperature

Further analysis considering different sea temperatures:

- Combined with seasonal metocean conditions, the operational current range obtained in this study can benefit engineers and practitioners in adjusting daily operational currents flowing through the cable core.
- Example using sea temperature data from Penzance and St. Ives (closest station to Cornish development zone).

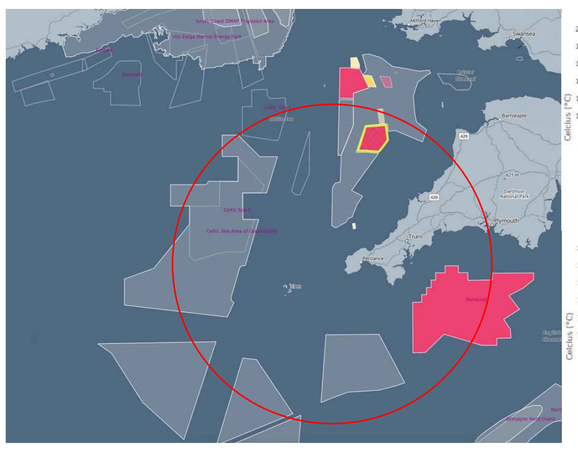

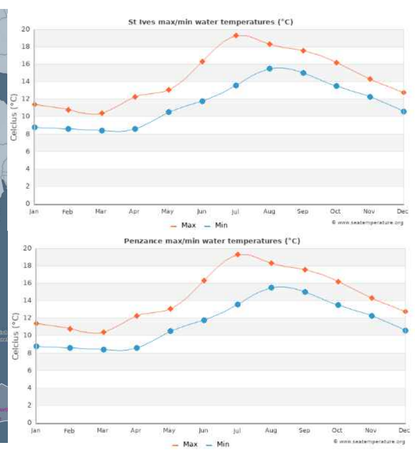

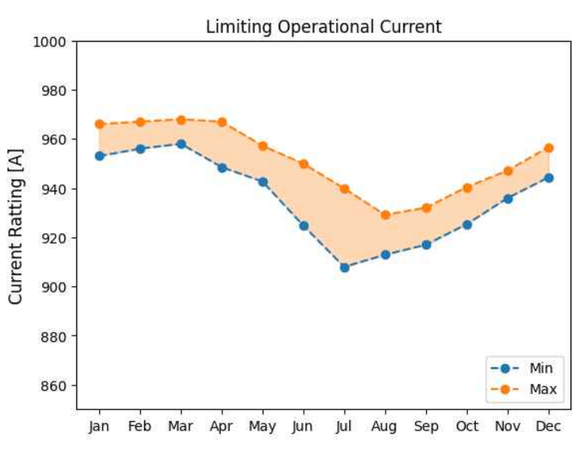

Adaptive operational strategy for offshore wind farm

Further Works:

- Cable behaviour under environmental loading at different temperature levels.
- Cable behaviour under the influence of external heating sources.

Acknowledgment:

The authors would like to thank Fulgor Single Member S/A. Hellenic Cable Industry for their financial support of this work through a funded PhD studentship with the University of Exeter.

A.C. Pillai acknowledges support from the Royal Academy of Engineering under the Research Fellowship scheme (award number: RF\202021\20\175).

HELLENIC CABLES
Member of CENERGY HOLDINGS

References:

[1] M. U. T. Rentschler, F. Adam, P. Chainho, K. Krügel, and P. C. Vicente, "Parametric study of dynamic inter-array cable systems for floating offshore wind turbines," *Marine Systems and Ocean Technology*, vol. 15, no. 1, pp. 16–25, Mar. 2020, doi: 10.1007/s40868-020-00071-7.
[2] J. Yang, Y. Zhang, and Y. Bai, "Electrothermal coupling analysis of submarine cables," *Ships and Offshore Structures*, 2024, doi: 10.1080/17445302.2024.2397295.
[3] J. Wang, H. Jin, Z. Yang, B. Zhao, X. Ma, and K. Ji, "Study on finite element analysis of the external heat resistance of cables in ductbank," in *Energy Reports*, Elsevier Ltd, Feb. 2020, pp. 322–329. doi: 10.1016/j.egyr.2019.11.083.
[4] M. Rachek and S. N. Larbi, "Magnetic eddy-current and thermal coupled models for the finite-element behavior analysis of underground power cables," *IEEE Trans Magn*, vol. 44, no. 12, pp. 4739–4746, Dec. 2008, doi: 10.1109/TMAG.2008.2004212.
[5] K. Grivas, A. Moraiti, G. Georgallis, G. Rinaldi, P. R. Thies, and L. Johanning, "Dynamic HV cables with AL conductors for floating offshore wind turbines: a cost and behavior comparative study," 2020.
[6] R. Østerø, J. Holbøll, R. Olsen, E. Dk Denmark, and I. A. Aristi, "Critical Conductor Temperatures in Submarine Cables Equipped with Protection Pipes," 2015.
[7] M. Á. González-Cagigal, J. C. Del-Pino-López, A. Bachiller-Soler, P. Cruz-Romero, and J. A. Rosendo-Macías, "Article a thermal model for three-core armored submarine cables based on distributed temperature sensing," *Energies (Basel)*, vol. 14, no. 13, Jul. 2021, doi: 10.3390/en14133897.
[8] A. Matine, E. Schaeffer, and C.-H. Bonnard, "Investigation of the biofouling thermal effects on offshore wind turbine power cables," in *10th International Conference on Insulated Power Cables*, 2019.
[9] Z. Maksassi, B. Garnier, A. O. El Moctar, F. Schoefs, and E. Schaeffer, "Thermal Characterization and Thermal Effect Assessment of Biofouling around a Dynamic Submarine Electrical Cable," *Energies (Basel)*, vol. 15, no. 9, May 2022, doi: 10.3390/en15093087.
[10] C. Petersen, "Around the North Sea." Accessed: Apr. 24, 2025. [Online]. Available: https://europe.oceana.org/blog/around-north-sea/
[11] C. Everard and C. F. Wooldridge, "English Channel," *Encyclopedia Britannica*. 2025. Accessed: Apr. 24, 2025. [Online]. Available: https://www.britannica.com/place/English-Channel
[12] E. Ruiz-Castillo, J. Sharples, J. Hopkins, and M. Woodward, "Seasonality in the cross-shelf physical structure of a temperate shelf sea and the implications for nitrate supply," *Prog Oceanogr*, vol. 177, Oct. 2019, doi: 10.1016/j.pocean.2018.07.006.
[13] "Baltic Marine Environment Protection Commission Baltic Sea Environment Proceedings 155 Baltic Sea-Second HELCOM holistic," 2011. [Online]. Available: www.helcom.fi/baltic-sea-trends/holistic-assessments/state-of-the-baltic-sea-2018/reports-and-materials/
[14] B. Boxer and M. Salah, "Mediterranean Sea," *Encyclopedia Britannica*. 2025. Accessed: Apr. 24, 2025. [Online]. Available: https://www.britannica.com/place/Mediterranean-Sea
[15] J. Zhu, J. Hu, and Q. Zheng, "An overview on water masses in the China seas," Aug. 22, 2022, *Frontiers Media S.A.* doi: 10.3389/fmars.2022.972921.
[16] H. Zhou, R. Zeng, B. Cong, Q. Jiang, and Z. Zhang, "Spatiotemporal distribution of sedimentary chloropigments and organic carbon in a shelf sea ecosystem, with a focus on the cold water mass," *Marine Development*, vol. 2, no. 1, p. 25, Oct. 2024, doi: 10.1007/s44312-024-00038-x.
[17] H. Nakahara and K. Senpaku Building, "Global Warming and the Circulation in the Sea of Japan," 2000.
[18] M. Fava, "Atlantic Ocean basin: a Detailed Map," Ocean Literacy Portal. Accessed: Apr. 24, 2025. [Online]. Available: https://oceanliteracy.unesco.org/atlantic-ocean/
[19] *INTERNATIONAL STANDARD Electric cables-Calculation of the current rating-Part 1-1: Current rating equations (100 % load factor) and calculation of losses-General*. 2023. [Online]. Available: www.iec.ch
[20] *INTERNATIONAL STANDARD Electric cables-Calculation of the current rating-Part 2-1: Thermal resistance-Calculation*. 2023. [Online]. Available: www.iec.ch
[21] A. Matine and M. Drissi-Habti, "On-coupling mechanical, electrical and thermal behavior of submarine power phases," *Energies (Basel)*, vol. 12, no. 6, 2019, doi: 10.3390/en12061009.
[22] *IEC Technical Report 62095-IEC TR 62095:2003-Electric cables - Calculations for current ratings - Finite element method*, vol. 1.0. 2003.
[23] Z. Maksassi, A. Ould, E. L. Moctar, B. Garnier, F. Schoefs, and E. Schaeffer, "For better comprehension of mussel's thermal characteristics and their thermal effect on dynamic submarine electrical cables," 2024. [Online]. Available: https://www.elsevier.com/open-access/userlicense/1.0/

Structured porous media for scour mitigation around offshore foundations

Dr. Elias J. G. Arcondoulis

Lecturer, Institute of Sound and Vibration Research,
School of Engineering, University of Southampton

University of Southampton

Supergen Offshore Renewable Energy

What is scour & why is it a problem?

Scour is the **localised erosion** of sediment around a structure driven by flow-induced shear, vortex dynamics and pressure gradients that mobilise and **transport bed material**.

Local scour poses a major threat to the **structural integrity** and **operational life** of **floating wind turbine foundations**.

- over-conservative design
- costly maintenance
- remotely operated vehicle inspections

Two times more upfront and ongoing costs than fixed-bottom turbines

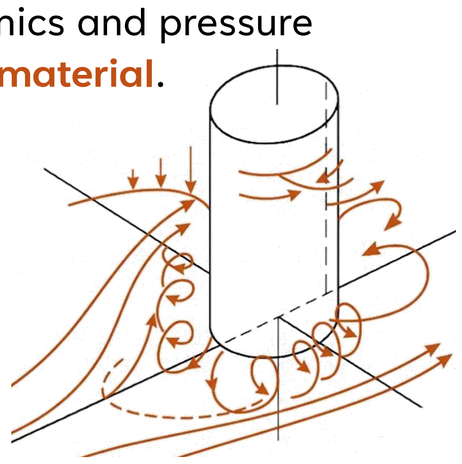

Scour flow physics
Adapted from [1]

How is scour currently treated?

Scour is typically treated mainly through **armouring-based protection measures**

(i) **rock riprap**

(ii) **mattresses**

(iii) **concrete units**

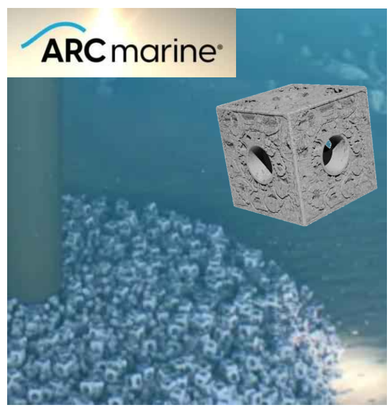

Aeroacoustics → Sediment hydrodynamics : Interdisciplinary concept?

Structured porous media (SPM)

- Applicable for flow and noise control of long, slender cylinders (e.g., aircraft landing gear) [4]
- Attenuates vortex shedding, near-wall recirculation & unsteady loading
- Reduces shear layer intensity
- > 1*D* additional total thickness

Can SPM be used to mitigate scour?

Untreated

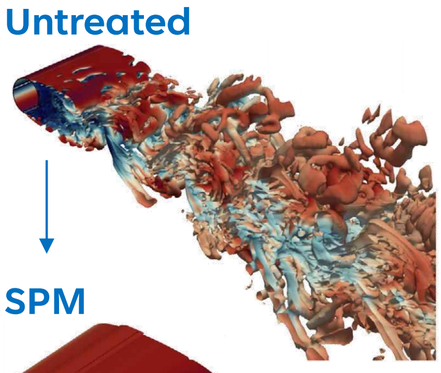

SPM

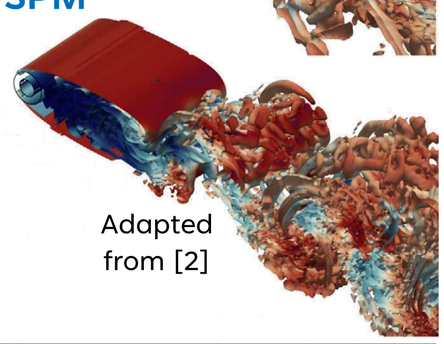

Adapted from [2]

Proprietary SPM results

$U_0 \approx 0.15$ m/s, $D = 41$ mm, $d_{50} = 180$ μm, $\theta \approx 0.02$

(I) Scour inception [$t^* = tU_0/D \sim O(10^2)$]

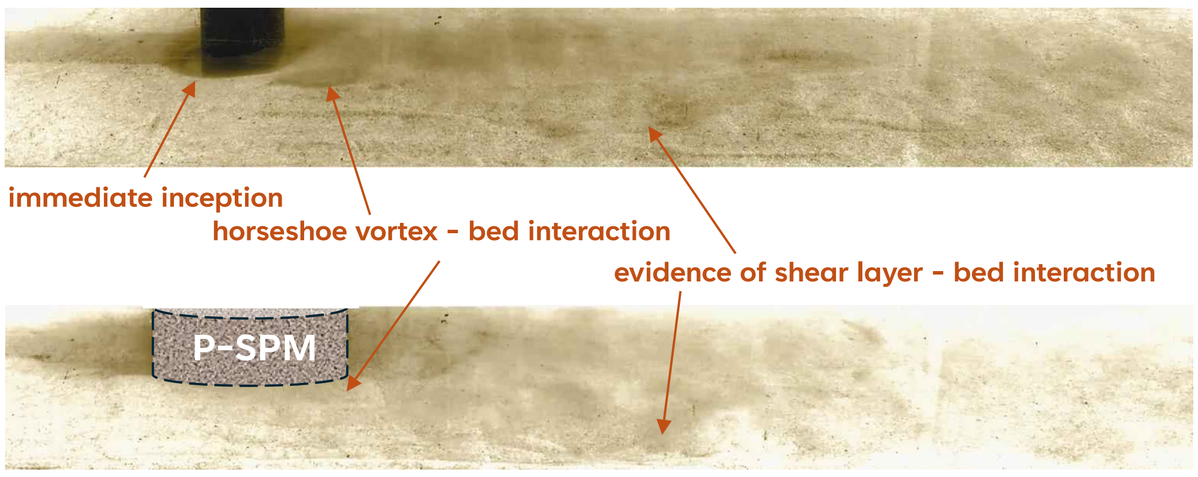

(II) Scour growth & edge scour initiation [$t^* \sim O(10^3)$]

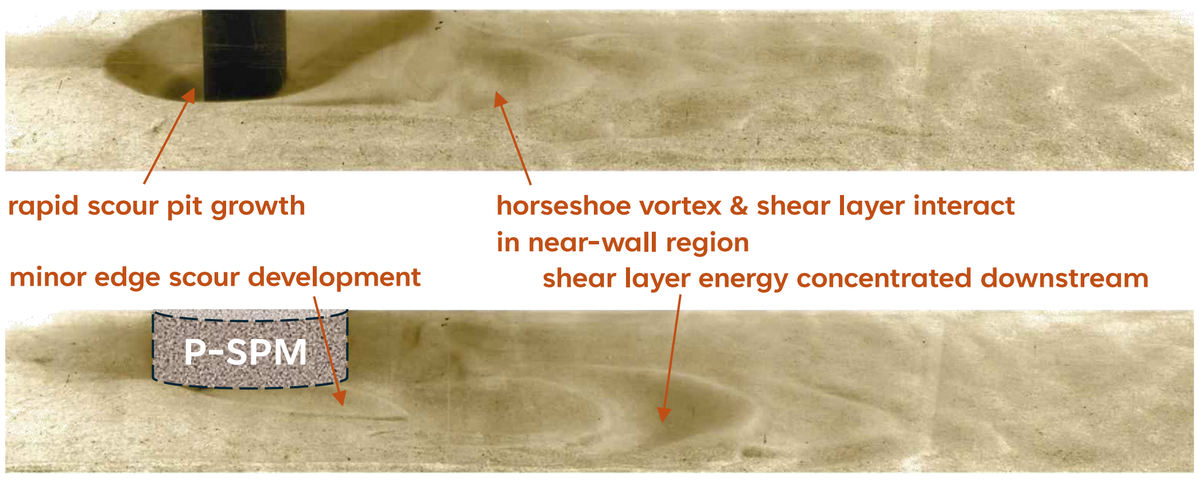

(III) Near-converged scour state [$t^* \sim O(10^4)$]

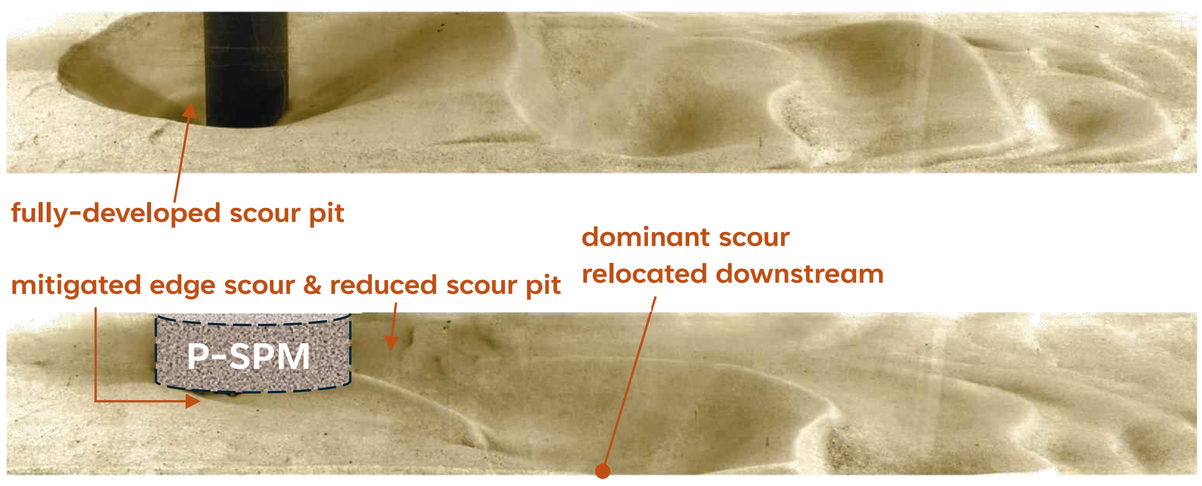

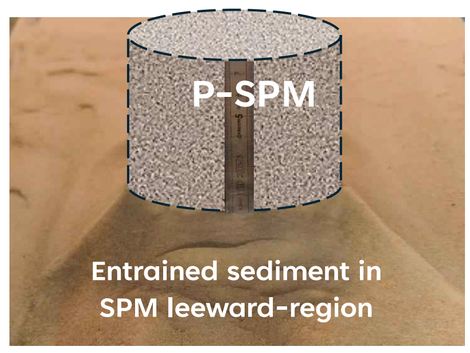

SPM substantially reduces scour depth at structure, edge scour initiation and promotes local sediment retention

Acknowledgements

This work was funded by the **Supergen ORE Hub – ECR Research Fund "ECRRF2025"**. I extend my sincere gratitude to **Dr. Hachem Kassem** & **Mr. Matthew Beverley-Smith** for their support and guidance during the experimental regimes at the NOC.

References

[1] Roulund, A., Sumer, B.M., Fredsøe, J. and Michelsen, J., 2005. *Numerical and experimental investigation of flow and scour around a circular pile*. **Journal of Fluid Mechanics**, 534, pp.351-401.

[2] Sharma, S., Geyer, T.F. and **Arcondoulis, E.J.G.**, 2023. *On the influence of porous coating thickness and permeability on passive flow and noise control of cylinders*. **Journal of Sound and Vibration**, 549, p.117563.

[3] Wen, K., **Arcondoulis, E.J.G.** et al., 2021. *Structure resolved simulations of flow around porous coated cylinders based on a simplified pore-scale model*. **Aerospace Science and Technology**, 119, p.107181.

[4] **Arcondoulis, E.J.G.** et al., 2023. *Internal shear layer and vortex shedding development of a structured porous coated cylinder using tomographic particle image velocimetry*. **Journal of Fluid Mechanics**, 967, p.A17.

Madison Asbury

Probabilistic Fatigue Life Assessment of Offshore Wind Structures Accounting for Manufacturing Imperfections

Supervisor(s): Professor Ali Mehmanparast , Dr Marc Seidel (Siemens)
Industrial Sponsor: Siemens Gamesa

University of Strathclyde, 204 George Street, Glasgow, G1 1XW
madison.asbury@strath.ac.uk

Background

- As Europe's offshore wind capacity targets **46 GW by 2030** early-generation turbines are reaching the end of their **20–25-year design life**.
- Deterministic models use large safety factors
- Finite Element models are complex compared to analytical models.
- The aim is to accurately assess fatigue risk to safely predict or extend the life of aging assets using a probabilistic framework.

Methodology

- **Data Collection and Verification:** Datasets were reconstructed from published figures using WebPlotDigitizer.
- **Data Filtering:** Data was filtered using polynomial fitting and slope thresholds. The remaining data were validated against BS EN ISO 12108:2018 criteria.

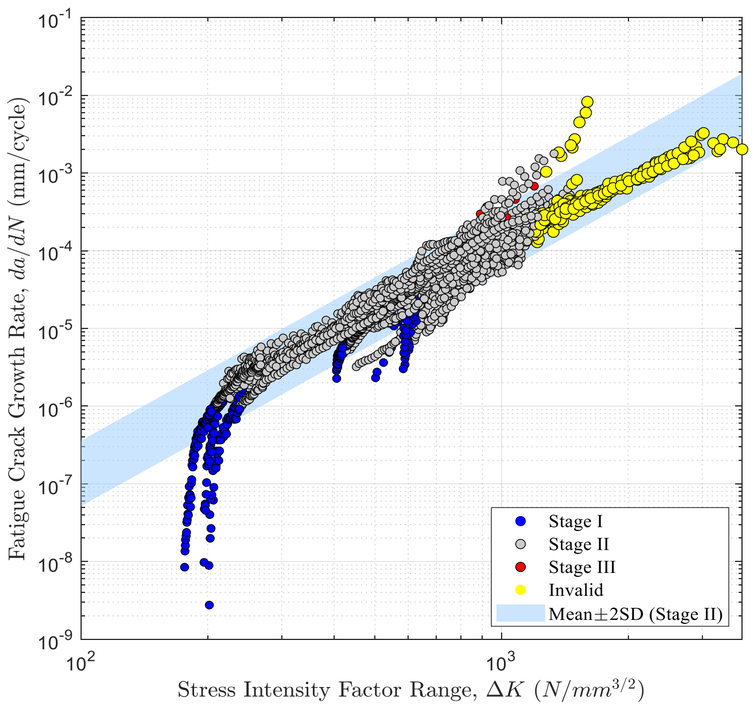

Figure 1: Fatigue crack growth data in air for 53 base metal and heat affected zone specimens separated into stage I, II and II crack growth. 0 ≤ R <0.5.

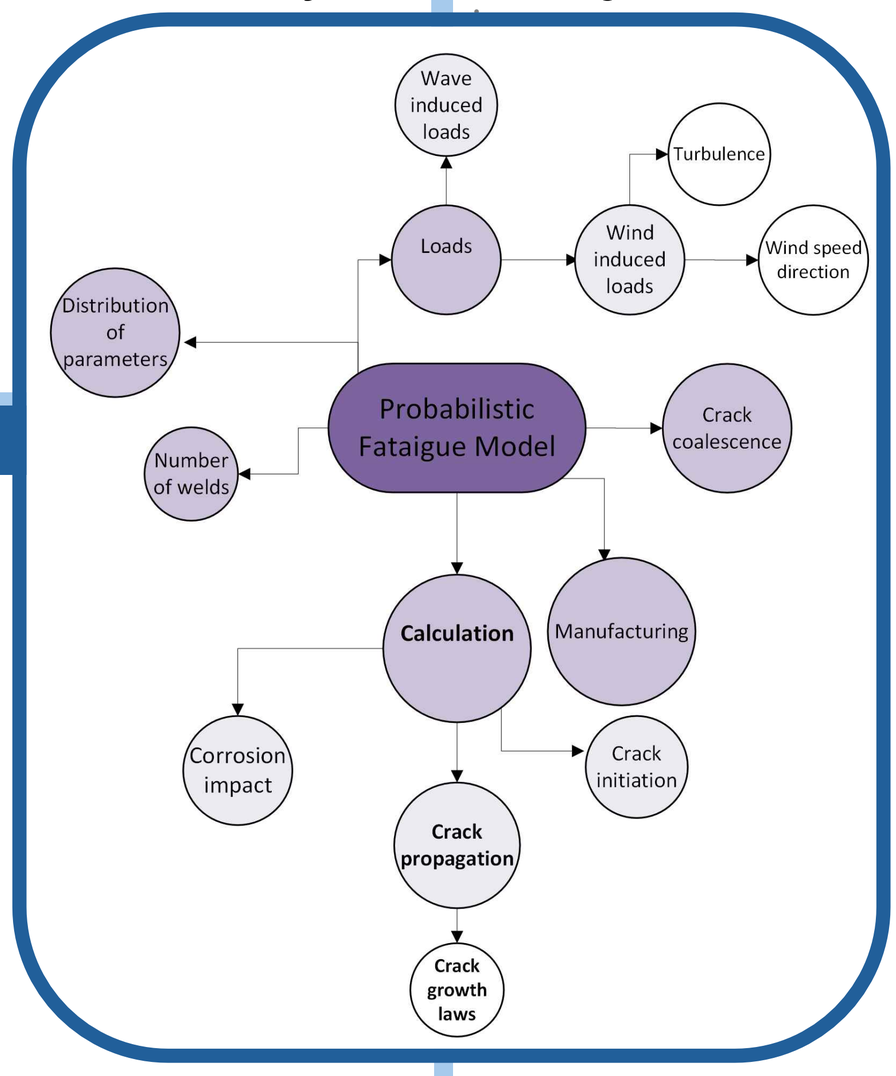

$$(W-a) \geq \left(\frac{4}{\pi}\right)\left(\frac{K_{max}}{R_{p0.2}}\right)^2$$

$$(W-a) \geq \left(\frac{3WF_{max}}{BR_{p0.2}}\right)^{0.5}$$

$$w_i = \frac{1}{n_{points}}$$

Results

- The S355 database does not show the distinct bilinear slope change assumed in BS 7910

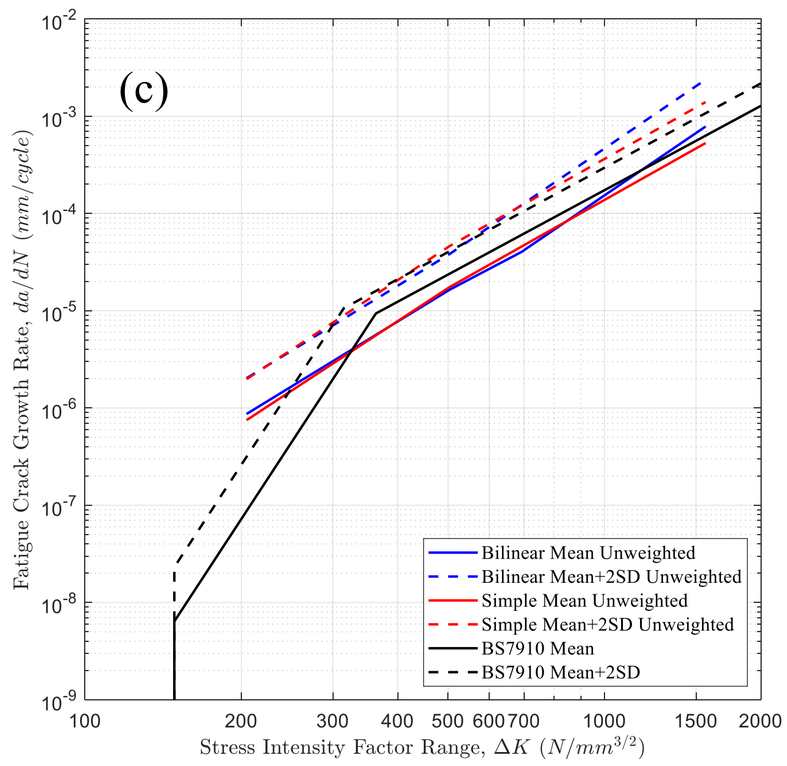

Figure 2: Bilinear and simple Mean and Mean+2SD curves compared with BS7910 bilinear fatigue crack growth curve in air for positive R < 0.5 using an unweighted approach.

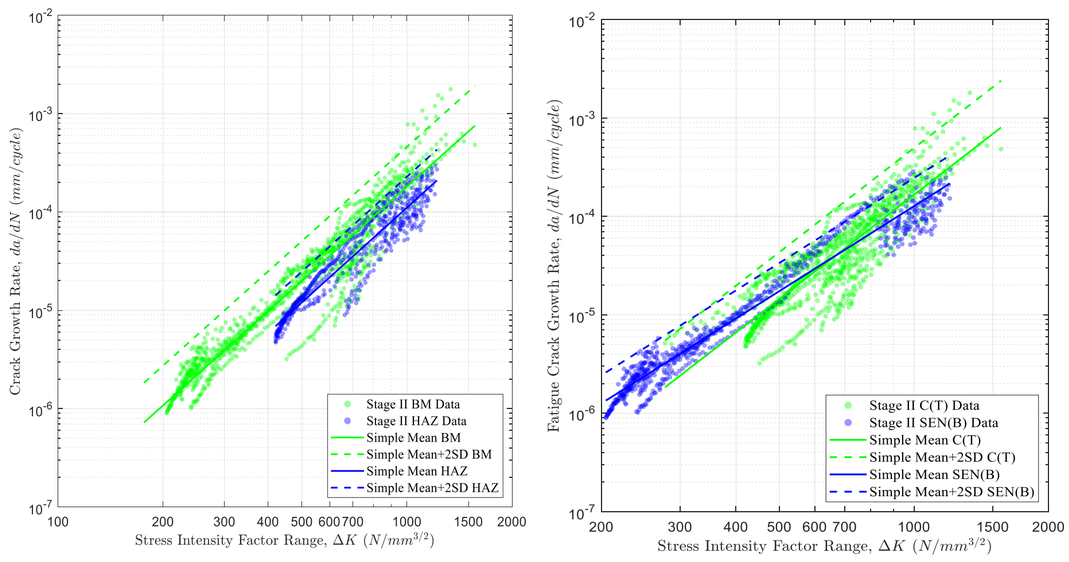

Figure 3: Linear regression Mean and Mean+2SD comparison for a) BM and HAZ; b) C(T) and SEN(B).

Conclusions

- BS 7910 bilinear curve underestimates fatigue life in the operationally relevant regions of ΔK (200-300 N/mm$^{3/2}$).
- A simple linear Paris Law fit is a sufficient representation of modern S355 steel.
- Probabilistic modelling has potential replace overly conservative safety factors with statistical reality.

Future Work

- Future research needed to address the scarcity of data at high load ratios (R>0.5).
- Simple crack growth law to be used further in a whole probabilistic model
- Investigations are needed to understand how residual stress relaxation might naturally slow crack growth in welded structures

References

Giuseppe Constanzo and G. Brindley, *Latest wind energy data for Europe*, R. O'Sullivan, Editor. 2025, wind europe.
Spyroudi, A., *End-of-life planning in offshore wind* 2021, Offshore Renewable Energy Catapult.
Vorpahl, F., et al., *Offshore wind turbine environment, loads, simulation, and design.* WIREs Energy and Environment, 2013. **2**(5): p. 548-570.
Pakenham, B., A. Ermakova, and A. Mehmanparast A Review of Life Extension Strategies for Offshore Wind Farms Using Techno-Economic Assessments. Energies, 2021. 14, 1936 DOI: 10.3390/en14071936.
King, R.N., A review of fatigue crack growth rates in air and seawater. 1998, Health and Safety Executive: United Kingdom.
British Standards Institution., Guide to methods for assessing the acceptability of flaws in metallic structures. 2019.

University of Southampton | IROE INTELLIGENT & RESILIENT OCEAN ENGINEERING | Supergen Offshore Renewable Energy

Reliability-based design of offshore wind gravity foundations

Dr Abigail Bateman University of Southampton, UK, a.bateman@soton.ac.uk, https://www.southampton.ac.uk/iroe

Reliability-based design approach

Advantages:

- **Target probability** of failure chosen by designer.
- **Farm wide** probabilities available. If 1 foundation fails will others?
- Considers **soil strength and loading** uncertainty.

Approach – Probability Distributions:

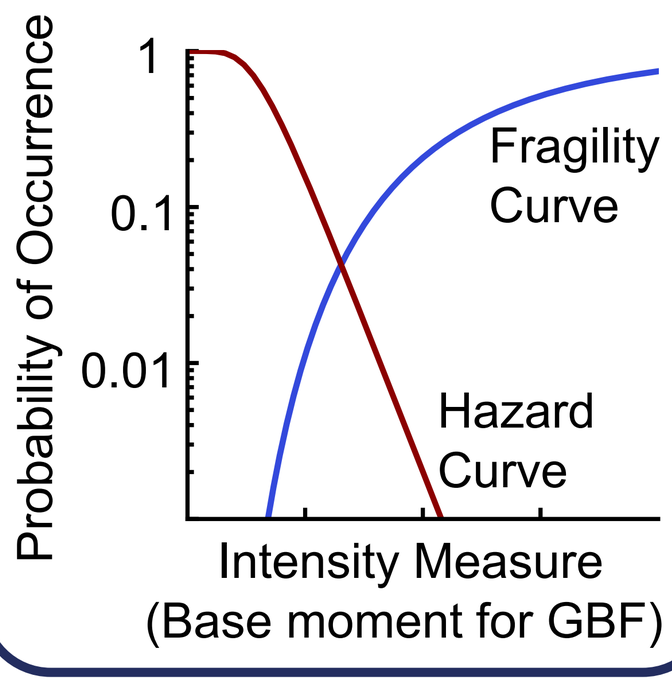

Three Example Sites: Different Strength Variability

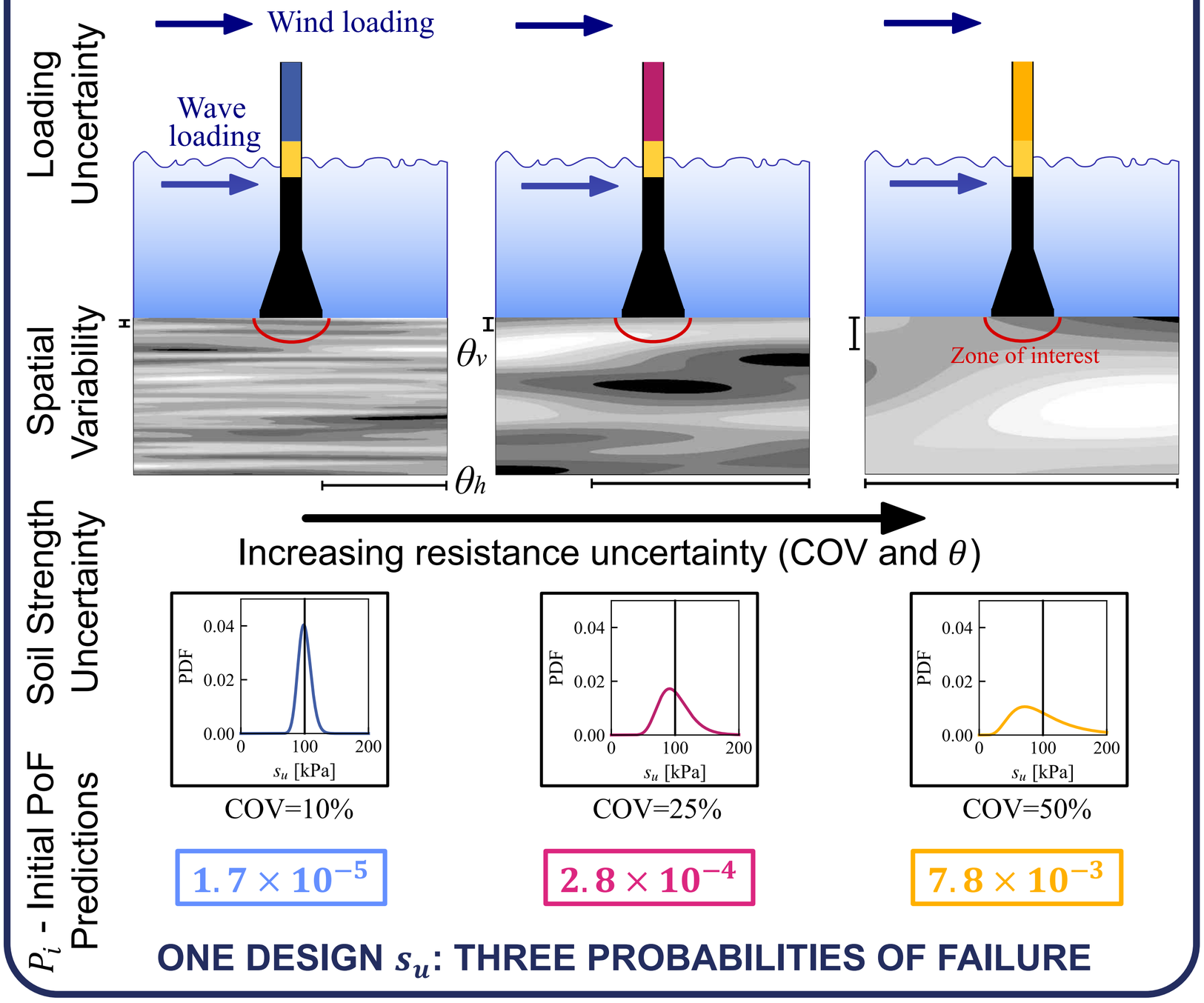

ONE DESIGN s_u: THREE PROBABILITIES OF FAILURE

Enhanced Analysis of Probability of Failure (PoF)

Combined Loading

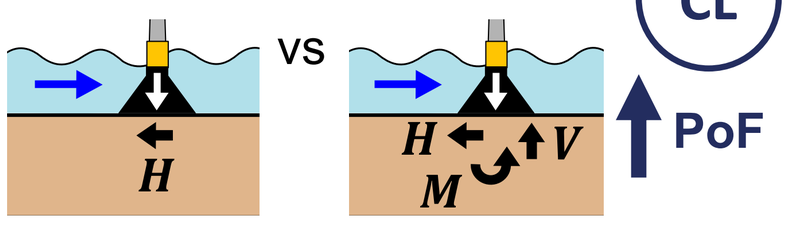

Spatial Averaging

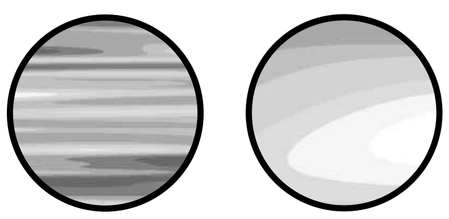

Long and Short Term Loading

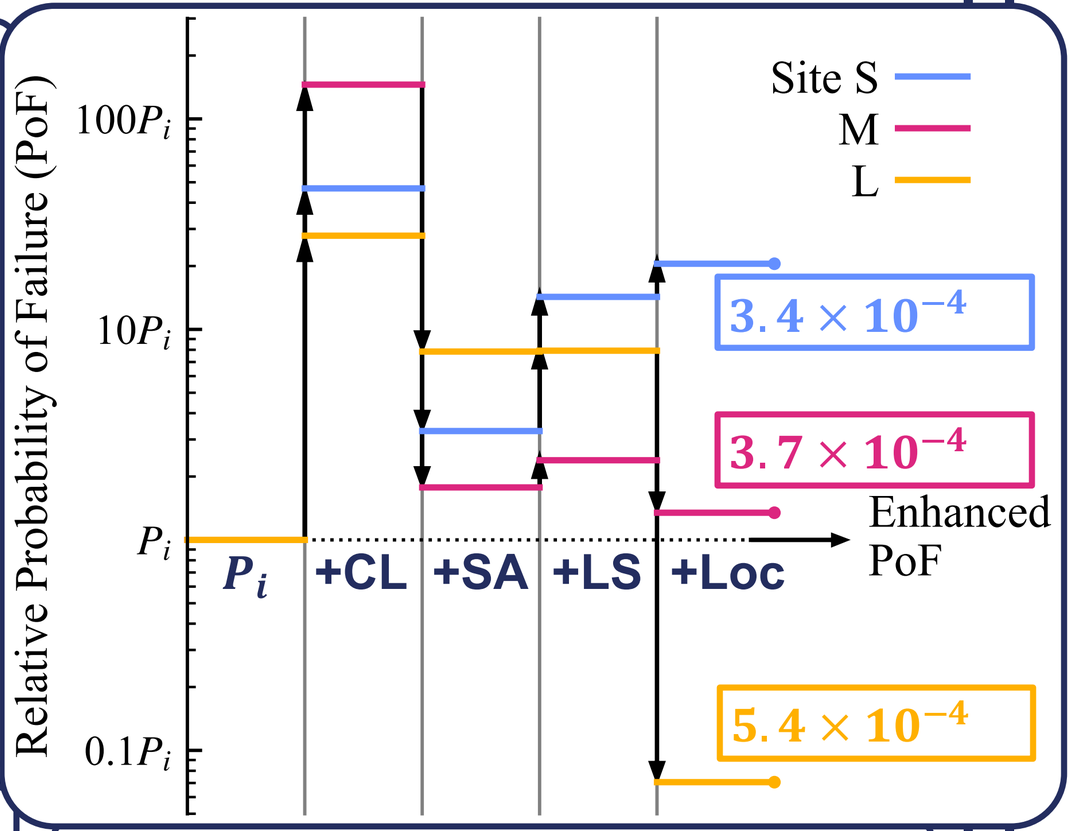

Location Specific Testing

Use local **Borehole/CPT** Not unit wide properties

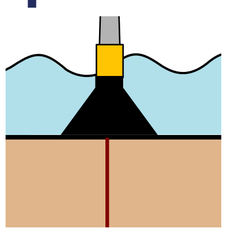

PoF

Loc

Implications

PoF calculation can be fast: new analytical methods

one design s_u + LRFD ≠ one PoF: COV and θ matter

Trust local CPT or use site-wide parameters? Depends on site variability

Acknowledgements: This work was supported by the EPSRC Supergen Offshore Renewable Energy Hub (grant EP/Y016297/1).

Supergen ORE Hub WS4: Response-conditioned short design events for floating ORE applications

Scott Brown[1,*], Tom Tosdevin[1], Jessica Guichard[2], Martyn Hann[2], Deborah Greaves[1]

[1]University of Oxford, Oxford, UK; [2]University of Plymouth, Plymouth, UK

**Corresponding email: scott.brown@eng.ox.ac.uk*

Aims and Objectives

- Are extreme responses from short design events comparable with traditional methods for floating ORE?
- Inform future best-practice guidelines for floating ORE.

What is a Short Design Event (SDE)?

A SDE is a **short duration** event that targets an **extreme response** from a device for given metocean conditions (Fig. 1).

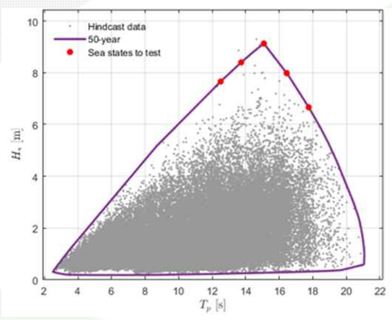

Figure 1: Metocean conditions example. Sea states are identified using a 50-year return period contour method[1].

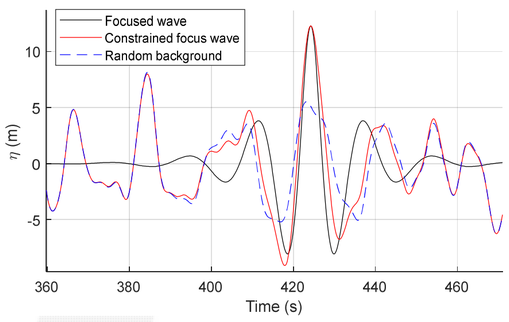

Figure 2: Example of a constrained SDE

SDEs may be either a wave, or a combined wind-wave profile. SDEs can be considered alone (**single** SDE) or embedded in a background wave (**constrained** SDE; see Fig. 2).

Supergen are developing "**response-conditioned**" SDE approaches (Fig. 3) where the profile is generated using an **RAO** to account for the **device's linear response**.

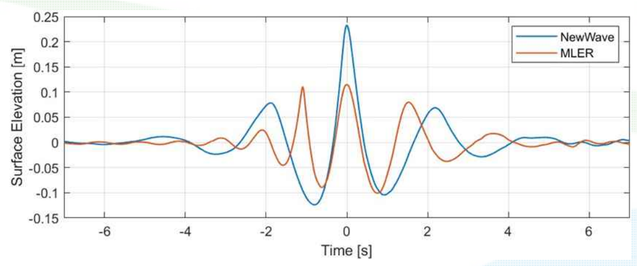

Figure 3: Comparison of a response-conditioned SDE (MLER) with a wave-height conditioned SDE (NewWave).

How does this differ from traditional design?

The traditional approach involves simulating **18-hours** (full scale) of irregular sea state (ISS) data. The data can be used to estimate exceedance probability, or the largest events averaged to provide a characteristic response.

This is relatively straightforward to implement but **time-consuming**. SDEs aim to provide an **efficient alternative.**

Methodology

We are primarily using scale physical modelling in the COAST Laboratory. Typical test plan:

1) Identify conditions that produce extreme response;
2) collect ISS and SDE data;
3) comparison of response for each method (Fig. 4).

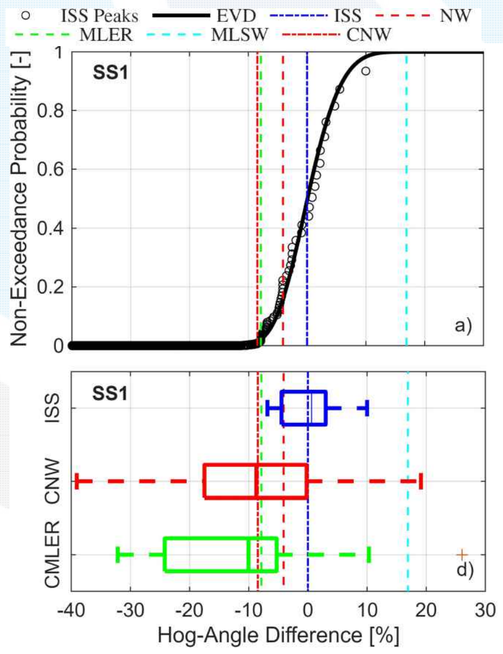

Figure 4: Example of a comparison of ISS and SDE methods for hog-angle of the Mocean Energy device (Fig. 5).

Wave Energy Update

Supergen have an ongoing collaboration with Mocean Energy. A 1:28 scale model of Mocean device (Fig. 5) has been used to evaluate SDEs for hog-angle and mooring load.

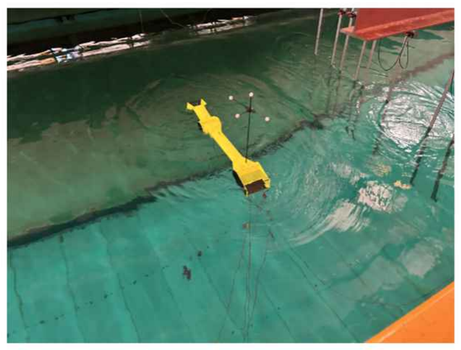

Figure 5: The Mocean Energy WEC model in the COAST Laboratory.

Observations

- Benefit of **response-conditioning limited** in this case
- Responses governed by **breaking waves**
- **Wave-steepness** conditioning performed best out of SDEs considered (with breaking point tuning)
- **Similar wave shapes** to hinged WECs tested previously.

Floating Offshore Wind Update

New physical models of the Windcrete spar for a 15MW turbine (Fig. 6) and a semi-sub for a 10MW turbine (Fig. 7) have been developed and used to assess SDEs. Responses have been extended to include tower base bending moment, with a flexible tower.

Figure 6: Scale model of the semi-sub in the COAST Laboratory.

Figure 7: Scale model of the Windcrete spar in the COAST Laboratory.

A real-time hybrid approach[2] (Fig. 7) is used where the aerodynamics are modelled using a thruster and an openfast-trained surrogate model. The aerodynamic system has been updated to improve communication time, and been expanded to a cut-out speed wind scenario.

Semi-sub Observations

- SDEs compare well with ISS data for **surge** and **mooring load**.
- **Pitch** agrees less than for VolturnUS[3]: needs further work.

Spar Observations

- Single SDEs perform well in **wind-driven** operational scenarios.
- **Constrained** SDEs required for tower base **moment** and **nacelle acceleration.**

References

[1] Tosdevin et al. (2025) On the development and application of short design events for the prediction of extreme responses of floating offshore wind turbines, Ocean Eng, 327, 120929.
[2] Ransley et al. (2023) Real-Time Hybrid Testing of a Floating Offshore Wind Turbine Using a Surrogate-Based Aerodynamic Emulator, ASME Open J. Engineering, 2, 021017.
[3] Brown et al. (2023) On the selection of design waves for predicting extreme motions of a floating offshore wind turbine, Ocean Eng., 290, 116400.

This work was supported by the Engineering and Physical Research Council (EPSRC) through funding from Supergen ORE Hub [EP/Y016297/1]. The physical models were developed through Supergen ORE Hub Early Career Researcher (ECR) funds for TT (spar) and JG (semi-sub). Additional funding sources were secured at the University of Plymouth for the development and testing of the semi-sub through an EPSRC impact acceleration account (IAA), and R&D Solutions Fund by Enterprise Solutions. The aerodynamic emulator updates were conducted in collaboration with the EPSRC project Integrated wind-wave control of semi-submersible floating offshore wind turbine platforms (FOWT-Control) [EP/W009692/1].